

## On-chip, photon-number-resolving, telecommunication-band detectors for scalable photonic information processing

Thomas Gerrits,<sup>1</sup> Nicholas Thomas-Peter,<sup>2</sup> James C. Gates,<sup>3</sup> Adriana E. Lita,<sup>1</sup> Benjamin J. Metcalf,<sup>2</sup> Brice Calkins,<sup>1</sup> Nathan A. Tomlin,<sup>1</sup> Anna E. Fox,<sup>1</sup> Antía Lamas Linares,<sup>1</sup> Justin B. Spring,<sup>2</sup> Nathan K. Langford,<sup>2</sup> Richard P. Mirin,<sup>1</sup> Peter G. R. Smith,<sup>3</sup> Ian A. Walmsley,<sup>2</sup> and Sae Woo Nam<sup>1</sup>

<sup>1</sup>*National Institute of Standards and Technology, Boulder, Colorado, 80305, USA*

<sup>2</sup>*Clarendon Laboratory, University of Oxford, Parks Road, Oxford OX1 3PU, United Kingdom*

<sup>3</sup>*Optoelectronics Research Centre, University of Southampton, Highfield SO17 1BJ, United Kingdom*

(Received 22 September 2011; published 5 December 2011)

Integration is currently the only feasible route toward scalable photonic quantum processing devices that are sufficiently complex to be genuinely useful in computing, metrology, and simulation. Embedded on-chip detection will be critical to such devices. We demonstrate an integrated photon-number-resolving detector, operating in the telecom band at 1550 nm, employing an evanescently coupled design that allows it to be placed at arbitrary locations within a planar circuit. Up to five photons are resolved in the guided optical mode via absorption from the evanescent field into a tungsten transition-edge sensor. The detection efficiency is  $7.2 \pm 0.5\%$ . The polarization sensitivity of the detector is also demonstrated. Detailed modeling of device designs shows a clear and feasible route to reaching high detection efficiencies.

DOI: [10.1103/PhysRevA.84.060301](https://doi.org/10.1103/PhysRevA.84.060301)

PACS number(s): 03.67.Hk, 42.79.Pw, 42.82.-m, 42.50.Dv

Photonics provides a promising path for building and using complex quantum systems for both exploring fundamental physics and delivering quantum-enhanced technologies in information processing, metrology, and communications. Currently, the only feasible route toward sufficient complexity is integration, due to the high density of optical modes that can be contained within a single device and the extraordinary level of control that can be exercised over them. Although much research has gone into developing integrated elements at telecom wavelengths for classical applications, their use in the quantum regime has been limited, in large part because of intrinsic inefficiencies in input coupling, detector coupling, and propagation. The effect of these inefficiencies is to reduce or remove any quantum advantage attainable with a given device [1–7].

Current single-photon-sensitive detectors for telecom wavelengths include avalanche photodiodes (APDs) [8], superconducting nanowires [9], and transition-edge sensors (TESs) [10,11].  $\text{In}_x\text{Ga}_{1-x}\text{As}$  APDs, the only commercially available telecom-band, single-photon-sensitive detectors, suffer from high dark-count rates, whereas nanowire detectors have much lower dark-count rates, are extremely fast, and can have high quantum efficiencies comparable to those of  $\text{In}_x\text{Ga}_{1-x}\text{As}$  APDs [12]. In order to achieve high efficiencies with these normal incidence detectors, care must be taken to impedance match the incident field to the detector in order to avoid reflections of the optical signal. Moreover, normal incidence-detection schemes are intrinsically limited to monitoring the modes that emerge from the end facet of the device. As a result, inferring information about a quantum state or circuit element inside a device will only become more problematic as circuits move toward the complexities required to study effects beyond the scope of classical computational power [7,13,14]. Developing high-efficiency detectors that are compatible with these complex, high-density systems is therefore a critical enabling step for quantum photonics.

In this paper, we demonstrate the operation of a new concept for broadband, efficient, single-photon detection, evanescently

coupled photon-counting detectors (ECPCDs), by merging two well-established technologies: photonic circuits and photon-number-resolving TESs. ECPCDs display the low noise and single-photon sensitivity required to operate in the quantum regime and, due to the evanescent coupling concept, are integration compatible, as they target a single guided mode at an embedded location within the circuit and maintain a fixed alignment. The photon absorber, in this case a tungsten TES, is placed in the evanescent field of the guided mode of a waveguide passing underneath the detector, as shown in Fig. 1(a). As the mode propagates through the detection region, it is coupled continuously into the detector via absorption. The continuous, evanescent coupling and the confinement of the waveguide mode allow potential for extended interaction regions, providing a straightforward way to increase efficiency even when the coupling is weak without limiting the detector acceptance bandwidth. A key feature of such a configuration is that the weak coupling allows use of a detector design that does not significantly modify the effective index and spatial profile of the guided mode, which minimizes reflections at the beginning of the detection region. The detector is therefore almost fully impedance matched. Finally, the lithographic construction makes this concept compatible with fabrication techniques for conventional telecom planar light-wave circuits, enabling sufficiently high detector densities to be useful with complex circuit designs.

In addition to the work presented here, two groups have recently implemented evanescently coupled superconducting nanowire single-photon detectors (SNSPDs) on Si and GaAs waveguided structures operating in the telecom band [15–17]. Even though the SNSPDs exhibit high dark-count rates compared with TESs and do not clearly resolve photon number, their speed allows for optical circuits with high photon count rates. Recently, the use of off-chip SNSPDs with waveguide quantum circuits has also been demonstrated [18].

TESs are sensitive detectors that use the electrical and thermal properties of a superconducting thin film to distinguish the energy of a discrete number of photons. They function

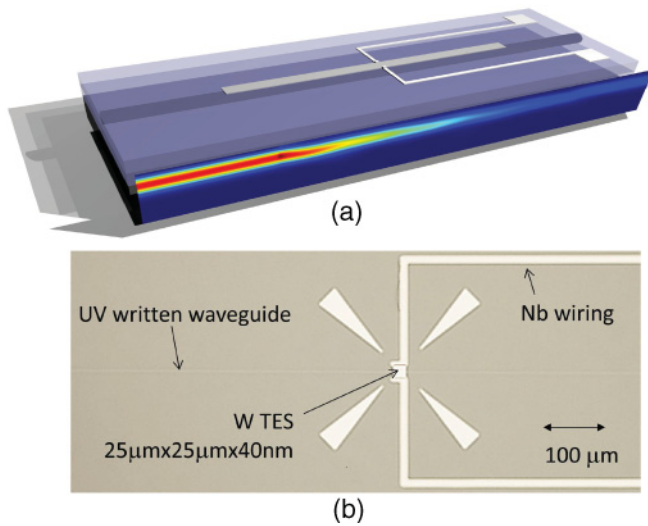


FIG. 1. (Color online) (a) Schematic of the evanescently coupled photon counting detector. The detection layer is deposited on top of an ultraviolet (UV) laser-written silica waveguide structure. The calculated internal mode profile can also be seen at the front of the device schematic. (b) Microscope image of the fabricated TES on the optical waveguide. The TES dimension is  $25\ \mu\text{m} \times 25\ \mu\text{m} \times 40\ \text{nm}$ . The tungsten TES bisects the waveguide in the center. The niobium wiring attaches to the top and bottom of the TES and exits off the chip to the right. Additional arrows simply serve as alignment marks and guide.

well across a very broad range of wavelengths and have been used to demonstrate the highest recorded detection efficiencies and number resolution, reaching 98% [19] and up to 10–30 photons depending on the design [10]. By positioning the material at its superconducting transition temperature  $T_c$  via voltage biasing, absorbed photons create a temperature change that can be measured via the resulting change in resistance [20]. To resolve this temperature change, the device's heat capacity must be carefully specified, which in turn limits the volume of superconducting material that may be used. The choice of detector geometry is therefore critical to ensure good energy resolution and high-efficiency absorption. In these first experiments to test the concept of a TES-based ECPCD, we chose detector dimensions of  $25\ \mu\text{m} \times 25\ \mu\text{m} \times 40\ \text{nm}$  [10], which has been shown to provide number resolution of tens of photons, while still exhibiting an easily accessible superconducting transition temperature.

Figure 2(a) shows the calculated absorption coefficient for the TE and TM modes of the waveguide as the thickness of a tungsten layer  $25\ \mu\text{m}$  wide is increased. This calculated absorption coefficient includes both the absorption in the tungsten TES and leakage from the propagating mode, as our modeling does not discriminate between them. A clear peak in the absorption coefficient for the TM mode is visible at around 45 nm thick. Initially, the absorption coefficient increases, because of the increase in volume of absorbing material interacting with the propagating field, but as the layer thickness increases beyond the skin depth of tungsten and the field no longer penetrates through the layer, the guided mode begins to be pushed away from the tungsten and the total flow of energy into the tungsten starts to be reduced. Also shown is

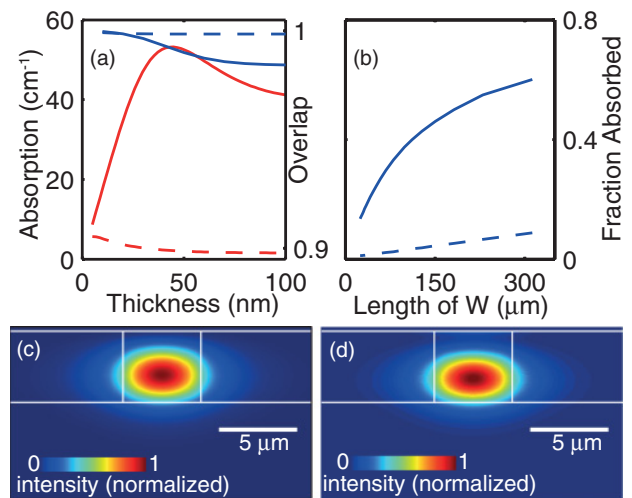


FIG. 2. (Color online) (a) Plot showing how the overlap between the mode supported by the regions with and without the detector (blue) and the absorption coefficient ( $\alpha/\text{cm}^{-1}$ , red) of both TE (dashed) and TM (solid) modes varies as the thickness of the layer is altered for a  $25\text{-}\mu\text{m}$ -wide detector. The maximum absorption coefficient for the TM mode occurs at around 45 nm, and the preferential absorption of the TM-like mode is clear. (b) Plot showing how the absorption for the TE (dashed) TM (solid) mode changes as the length of the detector is increased while keeping the volume constant at  $25\ \mu\text{m}^3$ . (c) The modeled normalized intensity distribution of the TM mode in the region without the detector. (d) The modeled normalized intensity distribution of the TM mode in the region with the detector for a 40-nm thickness. A slight distortion in the vertical direction can be seen along with a small amount of intensity near the detector layer.

the overlap of the TE and TM modes underneath the tungsten with those in the guide with no overlayer of tungsten, clearly demonstrating how little the spatial mode is perturbed by the presence of the detector. To test our model, a sample was fabricated with a  $100\text{-}\mu\text{m}$ -long, 40-nm-thick strip of tungsten across the waveguide. The measurements were done using a method described in Ref. [21]. The absorption coefficients for the TE and TM modes were measured to be  $3 \pm 2\ \text{cm}^{-1}$  and  $55 \pm 2.4\ \text{cm}^{-1}$ , which are in good agreement with our predicted values of  $2.3\ \text{cm}^{-1}$  and  $54.6\ \text{cm}^{-1}$ . Figure 2(b) shows the calculated absorption as the length and width of the detector are varied at 40 nm thick in order to maintain a constant volume of  $25\ \mu\text{m}^3$ . It can clearly be seen that absorption greater than 50% can be reached in a single device of this volume by employing a longer, narrower geometry. This could be further improved by either increasing the detector volume or fabricating a multiplexed array of devices.

For our test devices, the guiding structure was provided by a direct UV-written waveguide. These were produced by focusing a continuous-wave, 244-nm-wavelength laser into a  $5\text{-}\mu\text{m}$ -thick photosensitive layer of germanium-doped silica situated on top of an undoped silica layer and a silicon substrate. There are two key features of this waveguide platform for our devices. First, the top surface of the chip is smooth to less than 1 nm and is intrinsically planarized, which is critical, since surface roughness can suppress the tungsten superconducting transition temperature,  $T_c$ . Indeed, the observed  $T_c$  of  $\sim 90\ \text{mK}$  is in good agreement with the

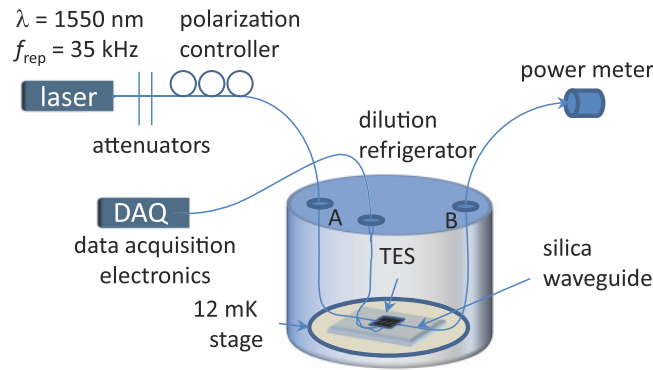


FIG. 3. (Color online) Experimental scheme. A 35-kHz pulsed laser at 1550 nm delivers attenuated weak coherent state pulses to the waveguide device, which is situated inside a dilution refrigerator. The input light's polarization can be modified via a fiber polarization controller. The waveguide device along with the TES is cooled to about 12 mK. The TES is voltage biased, and the electrical output is fed into a SQUID circuit (not shown). The SQUID output is amplified at room temperature, and the signal is measured with data acquisition electronics.

value we expect for a 40-nm-thick film of tungsten. Second, the guided mode is well mode matched to standard telecom fiber so that the device can be pigtailed with relatively low loss. Two TES detectors were fabricated, one positioned directly over the waveguide [as shown in Fig. 1(b)], and one 800  $\mu\text{m}$  away from it (not shown). The former is the main interest of this study, while the latter allowed the effects of scattered light to be observed.

A schematic of the experimental setup used to characterize the detectors is shown in Fig. 3. The device was pigtailed and glued at both input and output before being cooled to  $\sim 12$  mK in a commercial dilution refrigerator, significantly below the  $T_c$  for tungsten. Pigtailling both end facets of the device allowed us to test the loss in both directions and, by adjusting the input polarization, measure a total device throughput maximum of  $19.1 \pm 0.4\%$  and minimum of  $17.7 \pm 0.4\%$ , corresponding to TE and TM modes, respectively. The detectors were voltage biased within their superconducting transition region, and the electrical output of each was fed into a dc-superconducting interference device (SQUID) circuit (not shown). An electronically pulsed 1550-nm laser diode producing coherent states with 10 ns duration at  $\sim 35$  kHz was attenuated to a mean photon number of  $\langle n \rangle = 28.5 \pm 0.8$  per pulse by use of two calibrated fiber attenuators [22].

The raw output pulses of the central TES are shown overlaid on top of each other in Fig. 4(c), and a histogram of pulse heights is shown in Fig. 4(a) for the TM mode [the inset of Fig. 4(a) for the TE mode]. The clearly observable separation between pulse heights (the clearly resolved peaks in the histogram) demonstrates how well this detector can resolve photon number and shows that simple thresholding electronics are sufficient to determine the absorbed photon number. The measured mean photon number per pulse was  $0.986 \pm 0.02$  for the TM mode, found by optimizing the detector response while adjusting the input polarization. A mean photon number of  $0.086 \pm 0.008$  was found for the TE mode by adjusting the input polarization to the smallest detector response. We

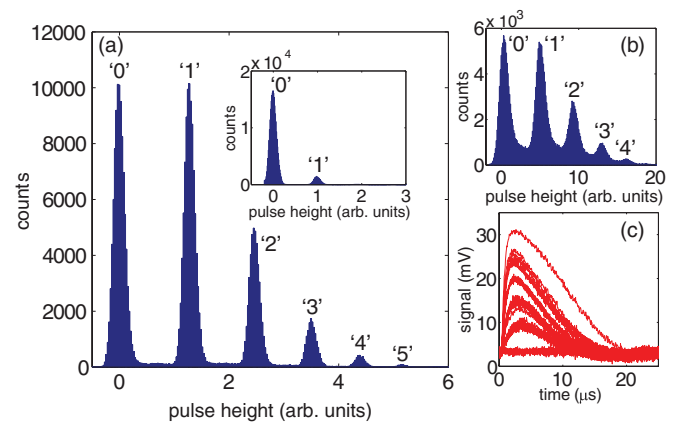


FIG. 4. (Color online) Experimental results. (a) Photon pulse height distribution for a measured coherent state with  $\langle n \rangle = 0.986$  for the optimal TM polarization ( $\eta_{\text{det}} = 7.2\%$ ). The inset shows the photon pulse-height distribution for the anti-optimal TE polarization. The measured mean photon number was 0.086 ( $\eta_{\text{det}} = 0.65\%$ ). (b) Photon pulse height distribution for the TES not evanescently coupled to the waveguide ( $\langle n \rangle = 1.03$ ;  $\eta_{\text{det}} = 0.0056\%$ ). (c) Electrical TES output traces for different numbers of photons in the weak laser pulse; the photon-number-resolving capability is clearly visible here. The TES recovery time is about 10  $\mu\text{s}$  due to its low transition temperature. Note that this detector was optimized for its photon-number-resolving capability and the evanescent coupling strength, not for its recovery time.

measured the photon number statistics and determined the mean photon number per pulse for both propagation directions to allow us to account for the effects of coupling and propagation loss [22]. This method yielded absolute detection efficiencies of  $7.2 \pm 0.5\%$  and  $0.65 \pm 0.05\%$  for the TM and TE modes, respectively. We compare this with our simulations, which predict absorption coefficients of 13.2% and 1.2% for our detector geometry. One possible explanation for this discrepancy is the fact that the model prediction does not discriminate between actual absorption of the tungsten TES and possible leakage of light from the waveguide structure, while the measurement provides only the absorption in the TES. In addition, fiber-splice losses in our system may also contribute to a measured detection efficiency a few percentage points lower than predicted [23].

Figure 4(b) shows a pulse-peak histogram for the reference detector after the input mean photon number was increased nominally by 32 dB and the input polarization was adjusted to obtain the maximum measured mean photon number. This number was  $1.03 \pm 0.02$ , implying a detection efficiency of 0.0056%, which we expect for a detector that measures only the scattered photon contribution. From the scattered light signal we estimate that this contribution to the central TES detection signal is  $\sim 8 \times 10^{-4}$  per pulse. The main peaks corresponding to direct photon number absorptions are still present; however, there are also intermediate pulse heights that contribute to an exponential tail on what is usually a Gaussian peak. We have evidence that these intermediate pulse heights are caused by a parasitic absorption of photons in the silica itself. An absorbed photon will create a cloud of hot electrons that couple to the silica phonon system. A part of this heat diffuses into the tungsten, causing a partial warm-up

(i.e., an energy collection efficiency lower than in the case of direct absorption) [24]. The effect is less pronounced in the central TES, as the majority of the photon absorption is due to evanescent coupling into the tungsten directly. We also observe a very small peak at half the photon energy, a possible indication of photon absorption in the niobium wiring [24]. We expect these effects to be suppressed when more optimized detector geometries with higher efficiency are used in the future.

In this Rapid Communication, we have realized the concept of an evanescently coupled photon-counting detector and demonstrated its operational feasibility by constructing a waveguide-based transition-edge sensor, the first implementation of an on-chip, truly photon-number-resolving-detector. We have shown a clear and realistic route to high-efficiency detection using this scheme by engineering the aspect ratio

of the detector. This wholly integrated solution for detection will be a key component of high-efficiency integrated devices functioning in the quantum regime. Such devices will be necessary in order to demonstrate technologies that show a palpable enhancement in functionality over their classical counterparts.

This work was supported by the NIST Quantum Information Initiative, the EPSRC (Engineering and Physical Sciences Research Council) (Grant No. GR/S82176/01) and EU IP (Integrated Project) Q-ESSENCE (Quantum Interfaces, Sensors, and Communication based on Entanglement). I.A.W. acknowledges the Royal Society. T.G. thanks Aaron J. Miller and M. Scott Bradley for discussions during the preparation of this manuscript. This material is a contribution of NIST, an agency of the US government, and is not subject to copyright.

- 
- [1] M. Varnava, D. E. Browne, and T. Rudolph, *Phys. Rev. Lett.* **97**, 120501 (2006).
- [2] M. Varnava, D. E. Browne, and T. Rudolph, *Phys. Rev. Lett.* **100**, 060502 (2008).
- [3] A. Politi, M. J. Cryan, J. G. Rarity, S. Yu, and J. L. O'Brien, *Science* **320**, 646 (2008).
- [4] A. Politi, J. C. F. Matthews, and J. L. O'Brien, *Science* **325**, 1221 (2009).
- [5] N. L. Thomas-Peter, B. J. Smith, A. Datta, L. Zhang, U. Dorner, and I. A. Walmsley, *Phys. Rev. Lett.* **107**, 113603 (2011).
- [6] A. Datta, L. Zhang, N. Thomas-Peter, U. Dorner, B. J. Smith, and I. A. Walmsley, *Phys. Rev. A* **83**, 063836 (2011).
- [7] N. L. Thomas-Peter *et al.*, *New J. Phys.* **13**, 055024 (2011).
- [8] J. Campbell *et al.*, *IEEE J. Sel. Top. Quantum Electron.* **10**, 777 (2004).
- [9] M. J. Stevens, R. H. Hadfield, R. E. Schwall, S. W. Nam, R. P. Mirin, and J. A. Gupta, *Appl. Phys. Lett.* **89**, 031109 (2006).
- [10] A. J. Miller, S. W. Nam, J. M. Martinis, and A. V. Sergienko, *Appl. Phys. Lett.* **83**, 791 (2003).
- [11] A. E. Lita, A. J. Miller, and S. W. Nam, *Opt. Express* **16**, 3032 (2008).
- [12] S. Miki, T. Yamashita, M. Fujiwara, M. Sasaki, and Z. Wang, *Opt. Lett.* **35**, 2133 (2010).
- [13] A. Laing, A. Peruzzo, A. Politi, M. R. Verde, M. Halder, T. C. Ralph, M. G. Thompson, and J. L. O'Brien, *Appl. Phys. Lett.* **97**, 211109 (2010).
- [14] A. Peruzzo, A. Laing, A. Politi, T. Rudolph, and J. L. O'Brien, *Nat. Commun.* **2**, 224 (2011).
- [15] A. Fiore *et al.*, in *Quantum Electronics and Laser Science Conference* (Optical Society of America, Baltimore, MD, 2011), p. PDPC3.
- [16] J. P. Sprengers *et al.*, *Appl. Phys. Lett.* **99**, 181110 (2011).
- [17] W. Pernice, C. Schuck, O. Minaeva, M. Li, G. Goltzman, A. Sergienko, and H. X. Tang, (2011), e-print arXiv:1108.5299 [quant-ph].
- [18] C. M. Natarajan, A. Peruzzo, S. Miki, M. Sasaki, Z. Wang, B. Baek, S. Nam, R. H. Hadfield, and J. L. O'Brien, *Appl. Phys. Lett.* **96**, 211101 (2010).
- [19] D. Fukuda, G. Fujii, T. Numata, K. Amemiya, A. Yoshizawa, H. Tsuchida, H. Fujino, H. Ishii, T. Itatani, S. Inoue, and T. Zama, *Opt. Express* **19**, 870 (2011).
- [20] K. D. Irwin, *Appl. Phys. Lett.* **66**, 1998 (1995).
- [21] H. L. Rogers, S. Ambran, C. Holmes, P. G. R. Smith, and J. C. Gates, *Opt. Lett.* **35**, 2849 (2010).
- [22] See Supplemental Material at <http://link.aps.org/supplemental/10.1103/PhysRevA.84.060301> for technical details of the experimental setup, the determination of the detection efficiency and our modeling.
- [23] A. J. Miller, A. E. Lita, B. Calkins, I. Vayshenker, S. M. Gruber, and S. W. Nam, *Opt. Express* **19**, 9102 (2011).
- [24] B. Cabrera, R. M. Clarke, P. Colling, A. J. Miller, S. Nam, and R. W. Romani, *Appl. Phys. Lett.* **73**, 735 (1998).